



## Synthesis of nickel nanoparticles using Plant Leaves and their application in the degradation of Pollutants

S. Subramani<sup>1</sup>, D. Thirumalai<sup>1</sup>, K. Sarumathy<sup>2</sup>, T. Vijay<sup>3\*</sup>

<sup>1</sup>Department of Chemistry, Thiruvalluvar University, Vellore(TN) - 632 115, India

<sup>2</sup>Tamil Nadu Pollution Control Board, Guindy, Chennai, (TN) – India

<sup>3</sup>Mercury college of Arts & Science, Arakkonam – Vellore (TN) – India

**Abstract :** Nickel nanoparticles as an eco-friendly adsorbent was biosynthesized using *Raphanus sativus* (Radish) leaf extract. The physiochemical properties of green synthesized nickel nanoparticles (NiGs) were characterized by UV-Vis spectroscopy (UV-Vis), Fourier Transform Infrared Spectroscopy (FTIR), X-ray diffraction (XRD), Scanning Electron Microscope (SEM) and Transmission Electron Microscope (TEM). NiGs were used as adsorbent for the removal of dyes such as crystal violet (CV), eosin Y (EY), orange II (OR) and anionic pollutants nitrate ( $\text{NO}_3^-$ ), sulfate ( $\text{SO}_4^{2-}$ ) from aqueous solution. Adsorption capacity of NiGs was examined in batch modes at different pH, contact time, NiGs dosage, initial dye and pollutant concentration. The adsorption process was pH dependent and the adsorption capacity increased with increase in contact time and with that of NiGs dosage, whereas the adsorption capacity decreased at higher concentrations of dyes and pollutants. Maximum percentage removal of dyes and pollutants were observed at 40, 20, 30, 10 and 10  $\text{mg}\cdot\text{L}^{-1}$  initial concentration of CV, EY, OR,  $\text{NO}_3^-$  and  $\text{SO}_4^{2-}$  respectively. The maximum adsorption capacities in Langmuir isotherm were found to be 0.454, 0.615, 0.273, 0.795 and 0.645  $\text{mg}\cdot\text{g}^{-1}$  at pH 8, 3, 3, 7 and 7 for CV, EY, OR,  $\text{NO}_3^-$  and  $\text{SO}_4^{2-}$  respectively. The higher coefficients of correlation in Langmuir isotherm suggested monolayer adsorption. The mean energies ( $E$ ), 2.23, 3.53, 2.50, 5.00 and 3.16  $\text{kJ}\cdot\text{mol}^{-1}$  for CV, EY, OR,  $\text{NO}_3^-$  and  $\text{SO}_4^{2-}$  respectively, calculated from Dubinin-Radushkevich isotherm showed physical adsorption of adsorbate onto NiGs. Adsorption kinetics data was better fitted to pseudo-second-order kinetics with  $R^2 > 0.870$  for all dyes and pollutants. NiGs were found to be an effective adsorbent for the removal of dyes and pollutants from aqueous solution and can be applied to treat textile and tannery effluents.

**Keywords :** *Raphanus Sativus*, Nickel nanoparticles, Adsorption, Adsorbents, Dyes, Pollutants.

## Introduction

Discharges of hazardous dyes and chemicals from textile and tannery industries into water bodies are worrying for both toxicological and esthetical reasons [1]. The dyes in water bodies reduce light penetration and photosynthesis and also degrade to produce toxic products like carcinogens [2]. Chemical pollutants in water bodies include dissolved anionic substances namely sulfate, nitrate and phosphate [3]. These anionic pollutants impart change in pH that affects chemical and biological processes in water bodies. Without appropriate treatment these compounds can remain permanently in the environment [4]. Many physical, chemical and biological treatment methods have been proposed for the removal of dyes and hazardous chemicals from water. Efficiency and expense of these processes is not suitable and economical for a developing country like India. Adsorption is considered to be an effective, economical and efficient method for removal of hazardous dyes and chemicals from water [2]. Nickel oxide is considered as good adsorbent due to its chemical and magnetic properties [4]. Various adsorbents, such as nickel oxide nanoparticles-modified diatomite [5], modified diatomite [6, 7] and polyvinyl alcohol/titanium oxide [8, 9] were applied to adsorb dyes, aromatic compounds and heavy metals from the aqueous solutions respectively. Nickel oxide nanoparticles-modified diatomite was reported as a good choice for removal of basic red 46 dye from aqueous solution [5]. The plant extracts are widely used for metal nanoparticle synthesis as they are easily available, safe, nontoxic and have a broad variety of metabolites (phytochemicals) that aid in the reduction of metal ions quicker than the microbes mediated synthesis [6]. Goutam *et al.* [10] reported that aqueous leaf extract of *Raphanus Sativus* can act as both reducing and capping agent in synthesis of silver nanoparticles. The present study aims to investigate the NiGs adsorption capacity on major industrial dyes crystal violet (CV), eosin Y (EY), orange II azo (OR) dyes and anionic pollutants nitrate ( $\text{NO}_3^-$ ) and sulfate ( $\text{SO}_4^{2-}$ ). Effects of various parameters such as contact time, pH, adsorbent dosage and initial adsorbate concentration on adsorption processes were investigated by equilibrium and kinetic methods. The adsorption processes were analyzed by Langmuir, Freundlich and Dubinin–Radushkevich isotherm models. The rate of adsorption was investigated by Langergren's pseudo-first-order and Ho–McKay's pseudo-second-order kinetics model.

## Materials and Methods

### Materials

Fresh leaves of *Raphanus sativus* (Fig. 2) were collected from Vellore town, Tamilnadu, India and the taxonomic identification was done at Thiruvallur University, Vellore, Tamilnadu, India. Nickel nitrate, barium sulfate and potassium nitrate were purchased from S.D. Fine Chemicals Ltd., Mumbai, India. Crystal violet, eosin Y and orange II azo dyes were purchased from Sigma- Aldrich (St. Louis, MO, USA).

### Synthesis of nickel nanoparticles and characterization

Fresh leaves of *Raphanus sativus* were collected and washed thoroughly with running tap water and distilled water and it was shade dried at  $(25 \pm 1)$  °C for 3 days. Leaves were powdered by mechanical grinding and were sieved using a 15-mesh sieve. Thereafter the powder was washed with 2% HCl solution and was dried out for further use. The leaf extract was prepared by dissolving 1 g leaf powder in 50 ml double distilled water. The contents were shaken in a shaker for 2 h and the precipitates were removed by filtration [11]. The filtrate was used as extract for the synthesis of NiGs.

NiGs were synthesized by subjecting 10 ml of *Raphanus sativus* leaf extract with aqueous  $1 \text{ mmol} \cdot \text{L}^{-1}$   $\text{Ni}(\text{NO}_3)_2$  to the vigorous stirring, where the reaction lasted for 3 h at 60 °C. The solution was freeze-dried for 24 h to obtain dried powder of nanoparticles [11]. The resulting powder was stored at 4 °C until further use.

The absorption optical spectrum of NiGs was recorded using Shimadzu UV-2401 PC double beam spectrophotometer from the range between 300 and 600 nm at  $(25 \pm 1)$  °C.

The FTIR spectrum of NiGs was recorded with Nicolet380 FTIR spectrometer. The sample was prepared at 0.25 mm thickness as KBr pellets (1 mg in 100 mg KBr) and stabilized under reactive humidity before acquiring the spectrum. The spectrum was measured between 500 and 4000 nm for 32 scans.

The XRD measurement on powder sample of synthesized nickel nanoparticles were carried out ( $2\theta = 10^\circ - 80^\circ$  at  $25^\circ\text{C}$ ) using a diffractometer system (XPERT-PRO, PANalytical) equipped with Ni-filtered Cu K-Alpha1 radiation ( $k = 0.15406$  nm). The diffractometer was operated with  $0.47^\circ$  divergent and receiving slits at 40 kV and 30 mA. A continuous scan was performed with a step size of  $0.05^\circ$   $2\theta$  and a step time of 10.1 s. The crystallite domain size was calculated from the width of the XRD peaks using the Scherrer formula.

$$D = 0.94 \lambda / \beta \cos \theta \quad (1)$$

where  $D$  is the average crystallite domain size perpendicular to the reflecting planes,  $\lambda$  is the X-ray wavelength,  $\beta$  is the full width at half maximum (FWHM), and  $\theta$  is the diffraction angle.

Morphological examination of NiGs was performed by SEM. The sample was coated on copper grid and the microscopic analysis was conducted using a Quanta FEI 250, SEM operated at 5 kV.

TEM analysis was performed using JOEL Model 1200 FX under 80 kV power supply. Samples were prepared by placing drops of nickel nanoparticles suspension over carbon coated copper grid, extra solution was removed by blotting paper and allowing the solvent to evaporate with the help of critical point drier. An image was formed by the interaction of electron transmitted through the specimen.

**Figure 1 UV-Visible Spectrum of NiGs**

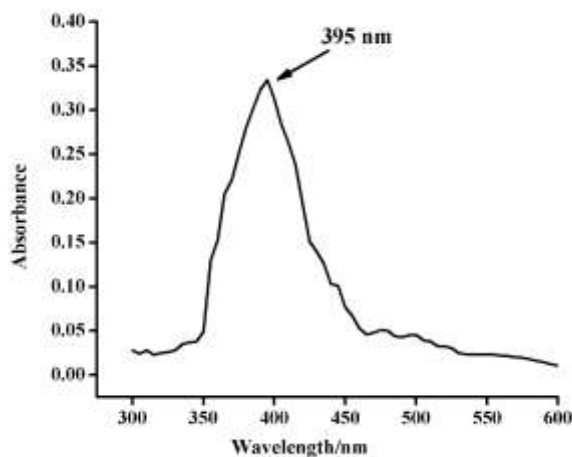
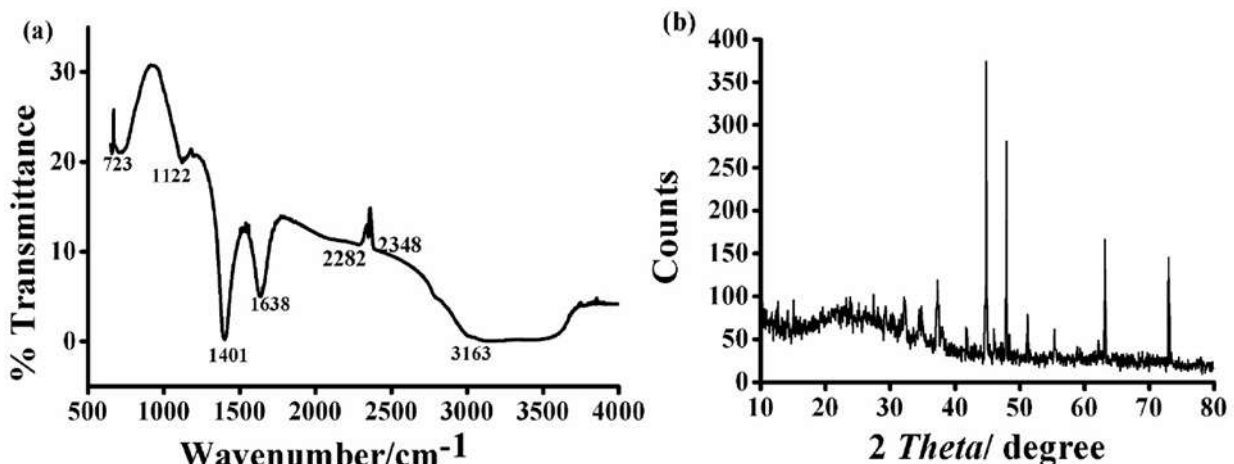


**Fig. 2. (a) FTIR spectrum and (b) X-ray diffraction pattern of NiGs**



## Batch experiments

Adsorption experiments were performed as batch modes. The pH of the dye and pollutant samples were adjusted with 0.1N NaOH or 0.1N HCl to obtain the desired pH value of 3–10. For each experiment, 0.1 g of NiGs was added to 100 ml of known concentration of dye or pollutant solution at  $(25 \pm 1)^\circ\text{C}$  and agitated at constant speed ( $150 \text{ r}\cdot\text{min}^{-1}$ ). The dye samples were collected and centrifuged at  $5000 \text{ r}\cdot\text{min}^{-1}$  for 10 min. The pollutant samples were filtered by pumping through both poly vinylidene fluoride membrane (pore size  $0.45 \mu\text{m}$ , microfiltration) and nylon membrane (pore size  $0.02 \mu\text{m}$ , ultra filtration) at  $1 \text{ ml}\cdot\text{min}^{-1}$  for complete removal of the nanoparticles. UV–Visible spectrophotometer (Shimadzu UV–2401 PC double beam spectrophotometer) was used to determine the concentration of dyes in the supernatant and nitrate pollutants in the filtrate. The absorbance at 590 nm (CV) [12], 520 nm (EY) [13], 500 nm (OR) [4] and 220 nm ( $\text{NO}_3^-$ ) [14] were used to calculate the equilibrium adsorption of the dyes and nitrate pollutants. The standard turbid-metric method [15] was used for the  $\text{SO}_4^{2-}$  analysis. The amount of dye or pollutant adsorbed per unit of NiGs was calculated using the Eq. (2) [16]:

$$q_e = (C_0 - C_t) V / W \quad (2)$$

where  $q_e$  ( $\text{mg}\cdot\text{g}^{-1}$ ) is the equilibrium dye and pollutant concentration onto NiGs,  $C_0$  ( $\text{mg}\cdot\text{L}^{-1}$ ) is initial dye or pollutant concentration,  $C_t$  ( $\text{mg}\cdot\text{L}^{-1}$ ) is the equilibrium concentration of dye or pollutant in solution,  $V$  (L) is the volume of experimental solution, and  $W$  (g) is the mass of NiGs. The removal percentage of dye and pollutant were calculated using the Eq. (3) [17]:

$$\text{Removal percentage} = (C_0 - C_e) / C_0 \times 100\% \quad (3)$$

where  $C_e$  ( $\text{mg}\cdot\text{L}^{-1}$ ) is the equilibrium concentration of dyes and pollutant.

## Adsorption studies

Equilibrium concentration in aqueous solution provides better perception of mechanism of adsorption process [8]. Langmuir, Freundlich and Dubinin–Radushkevich isotherm models were employed to examine the relationship between the amount of adsorbate ( $q_e$ ) and its concentration in aqueous phase ( $C_e$ ) at equilibrium at various contact time. The experimental data from various time intervals were used to analyze the adsorption isotherms.

## Kinetic studies

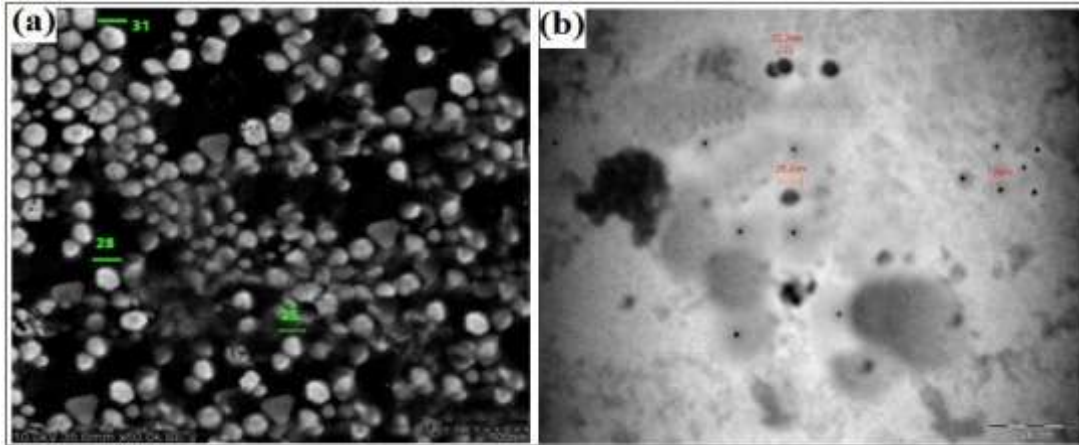
The rate of adsorption is important to design and evaluate the adsorbent in removing adsorbate from aqueous system. The Lagergren's pseudo-first-order kinetics [17] and Ho and McHay pseudo-second-order kinetics [18] models were used to investigate the experimental data.

## Results and Discussion

### Synthesis of nickel nanoparticles using aqueous leaf extract of *Raphanus Sativus*

In aqueous solution, nickel nitrate dissociates into negative nitrate anions and positive  $\text{Ni}^{2+}$  cations as given in the Fig. 3. The hydrated electrons from aqueous leaf extract of *Raphanus Sativus* reduce  $\text{Ni}^{2+}$  cations into zero valent nickel ( $\text{Ni}^0$ ) by nucleation process. Many  $\text{Ni}^0$  atoms agglomerate to form  $\text{Ni}_n^0$ . This phenomenon of agglomeration is due to the binding energy between two metal atoms which is stronger than the atom-solvent bond energy as previously reported for  $\text{Ag}_2^0$  by Kazem *et al.* [19] and for  $\text{Ni}_2^0$  by Abdo *et al.* [20]. Hence nickel atoms attract each other by diffusion while encountering progressively coalesce into the growing clusters by a cascade of coalescence processes, which is in good concurrence with earlier reports [19, 20].

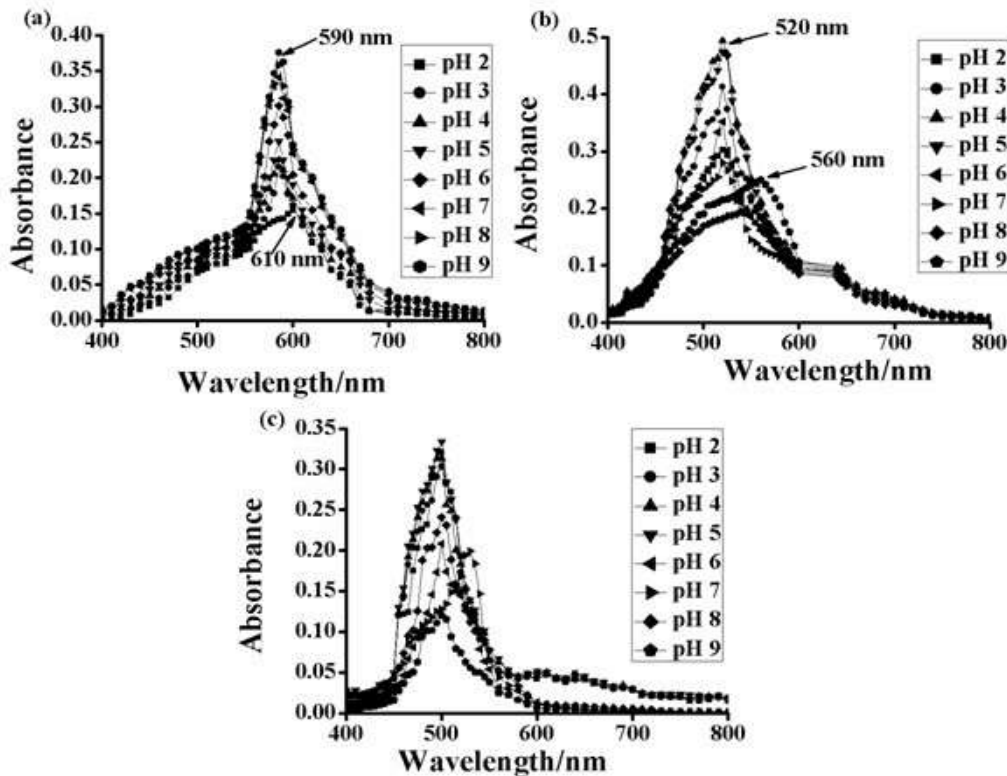
Fig. 3. (a) SEM and (b) TEM images of NiGs



**Characterization of synthesized NiGs**

The absorption spectrum of NiGs gives a peak centered at 395 nm (Fig. 4). UV–Vis spectroscopy curves and surface plasmon resonance (SPR) wavelength were sensitive to the characteristics of nanoparticles and the absorption spectra at 374 nm to 422 nm range corresponds to the SPR of nickel [21]. Related to our results, the presence of absorption peak at 395 nm shows the presence of nickel nanoparticles. The maximum wavelength and width of the SPR are mainly dependent of the size and shape of the nanoparticles [22]. The broadness of the bandwidth indicates the size of the nanoparticles. Therefore, increased bandwidth in the Fig. 4 evidences the presence of smaller particle size of nanoparticles.

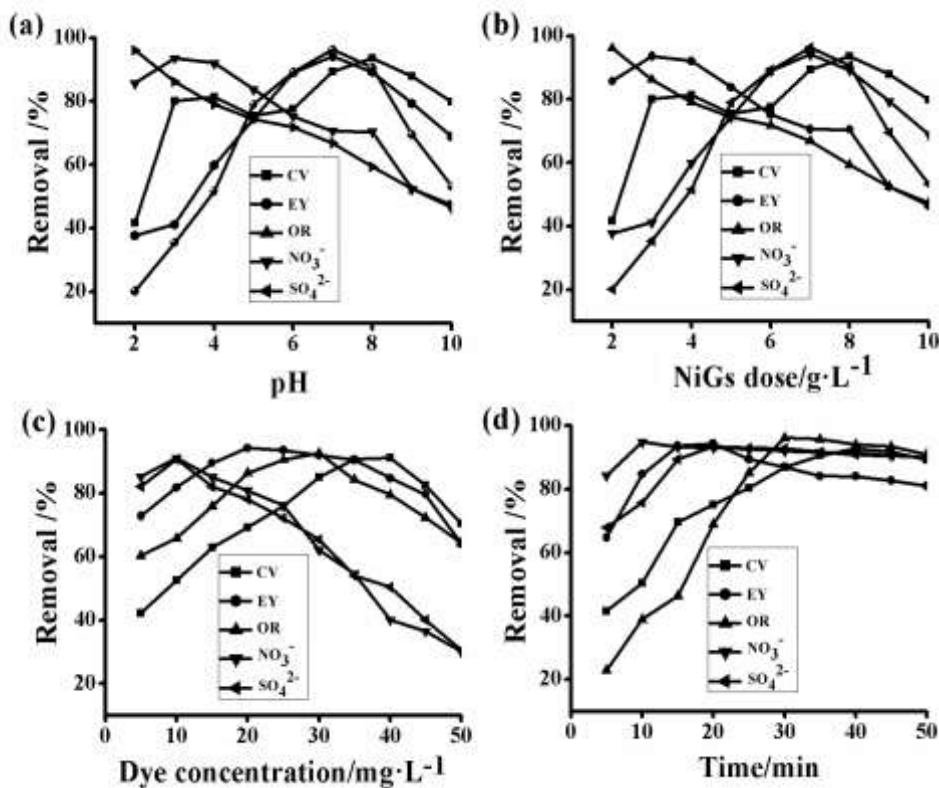
Fig. 4. UV–Vis absorption spectra of aqueous dyes (a) CV (b) EY and (c) OR at different pH Fig. 8. Effect of (a) pH, (b) NiGs dose, (c) initial dye or pollutant concentration and d) different contact time on removal of CV, EY, OR, NO<sub>3</sub><sup>-</sup> and SO<sub>4</sub><sup>2-</sup>.



FTIR analysis was carried out to identify the biomolecules for capping and efficient stabilization of the NiGs synthesized by *Raphanus sativus* leaf extract. The FTIR spectrum of synthesized NiGs is shown in the Fig. 5(a). The peak at  $3163\text{ cm}^{-1}$  corresponds to O–H stretching carboxylic acids. Characteristic peaks between  $2348$  and  $2282\text{ cm}^{-1}$  indicate the possible presence of C–N or C–C triple bonds. The peak at  $1638\text{ cm}^{-1}$  is attributed to N–H bend primary amines. The sharp peak at  $1401\text{ cm}^{-1}$  indicates C–C stretch (in ring) in aromatics. The peak at  $1122\text{ cm}^{-1}$  is primarily due to C–N stretching of aliphatic amines and the peak at  $723\text{ cm}^{-1}$  is characteristic of C–H rock in alkanes. The FTIR analysis evidences the presence of N–H, C–N, C–H and O–H groups, which corresponds to the presence of metabolites and proteins surrounding the NiGs. Mallikarjuna *et al.* [23] reported that the carbonyl and hydroxyl groups from amino acid residues or proteins can strongly bind to metal nanoparticles like capping agent and stabilize the nanoparticles by preventing its agglomeration. Sathyavathi *et al.* [24] also suggested that the biological molecules exhibit dual role of formation and stabilization of nanoparticles in the aqueous medium.

The XRD spectrum [Fig. 5(b)] display five distinct diffraction peaks at  $37.32^\circ$ ,  $44.82^\circ$ ,  $47.92^\circ$ ,  $63.11^\circ$  and  $72.97^\circ$ . The highest intensity for the peak observed was at  $2\theta$  value  $44.82^\circ$ . Their corresponding miller indices (111) and (200) confirm that the resulting powders were face-centered-cubic (fcc) nickel. The XRD pattern matches with the Joint Committee on Powder Diffraction Standards database (JCPDS PDF No.: 04 – 0850) that confirms the random powdered arrangement for nickel. The average particle size determined by Debye Scherrer equation was found to be 30 nm. The X–ray diffraction results clearly evidences that the nickel nanoparticles formed by the reduction of  $\text{Ni}^{2+}$  by *Raphanus sativus* leaf extract were crystalline in nature and this is in good agreement with the earlier report of Hou *et al.* [25].

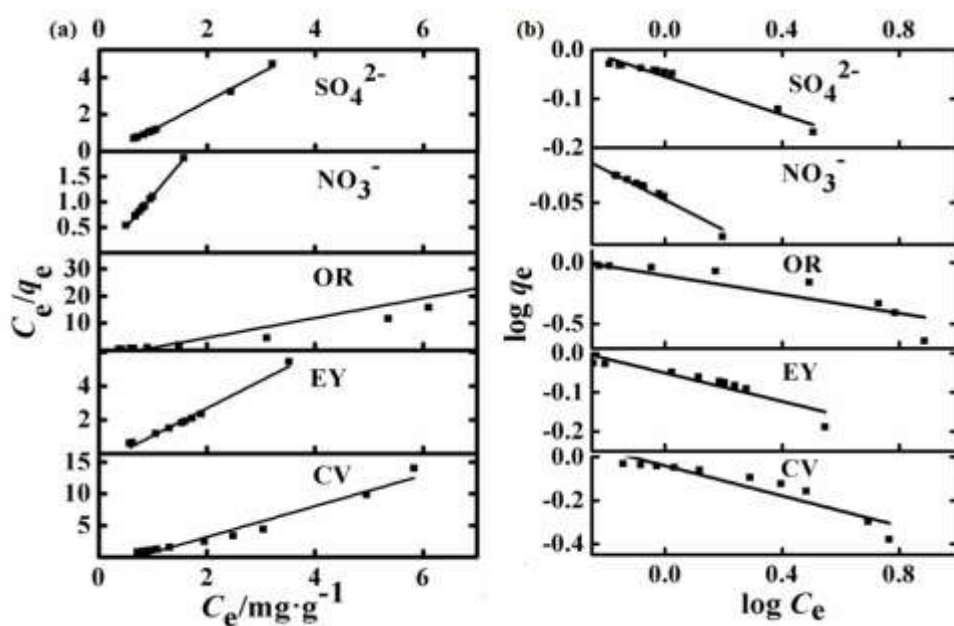
**Figure 5** Effect of (a) pH, (b) NiGs dose, (c) initial dye or pollutant concentration and d) different contact time on removal of CV, EY, OR,  $\text{NO}_3^-$  and  $\text{SO}_4^{2-}$ .



The SEM image of NiGs in the Fig. 6(a) show that the particles shape varied from spherical to polyhedral and the particle size ranged between 15 and 36 nm. According to Govindasamy *et al.* [26] the surface morphology of nickel nanoparticles were irregular polygonal, cylindrical and spherical in shapes. Hence the result obtained as crystalline in nature with size around 30 nm from the XRD analysis is in close agreement with the particle size observed in SEM.

The TEM image of the NiGs [Fig. 6(b)] shows that the shape of the NiGs was almost spherical in shape and the distribution of the particles was narrow. The diameter of the sample ranged between 12 and 36 nm and shows a certain extent of particles agglomeration. The agglomeration property of the nanoparticles is due to magnetic interaction and polymer adherence between the particles as reported earlier by Wang *et al.* [27].

**Figure 6 (a) Langmuir isotherm plot and (b) Freundlich isotherm plot for adsorption of CV, EY,OR, NO<sub>3</sub><sup>-</sup> and SO<sub>4</sub><sup>2-</sup> onto NiGs**



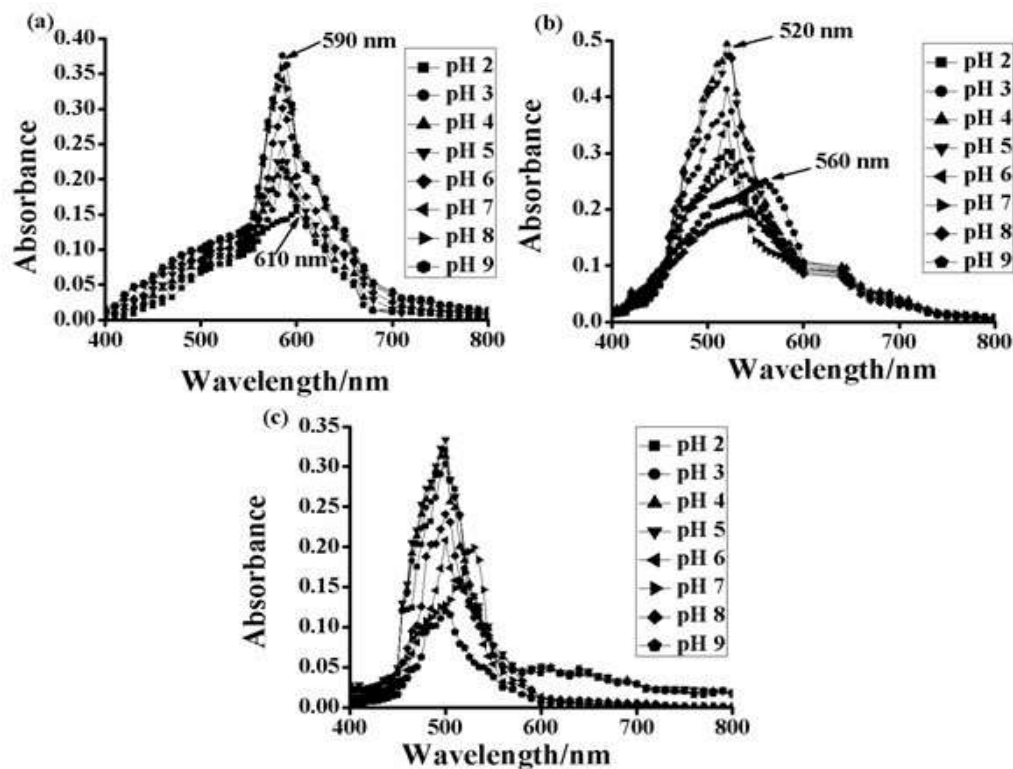
### Effect of pH

pH stability of dyes were observed from pH range between 2 and 9. UV-Vis absorption spectra of CV at different pH [Fig. 7(a)] show that the aqueous CV was stable in pH range between 3 and 9 with constant  $\lambda_{\max}$  590 nm. At pH 2, CV recorded  $\lambda_{\max}$  at 610 nm. Similarly absorbance of EY and OR [Fig. 7(b) and 7(c)] was stable in pH range between 2–7 and 2–8 with  $\lambda_{\max}$  at 520 nm and 500 nm respectively. At pH 9, EY and OR dyes recorded  $\lambda_{\max}$  at 560 nm and 530 nm respectively. On the basis of this  $\lambda_{\max}$  values all the further experiments were performed at 590 nm, 520 nm and 500 nm for CV, EY and OR respectively.

pH plays a vital role in aqueous chemistry and at surface binding sites of the adsorbents. The effect of pH (2–11) on the adsorption at  $(25 \pm 1)^\circ\text{C}$  with 10 mg NiGs in 10 ml of aqueous adsorbate solutions (CV–10 mg·L<sup>-1</sup>, EY–10 mg·L<sup>-1</sup> and OR–30 mg·L<sup>-1</sup>) for 30 min contact time is shown in the Fig. 8(a). For all the parameters, the percentage removal of dyes was evaluated by the Eq. (2). The optimum pH of the dyes (CV, EY and OR) was 8, 3 and 3 respectively. The optimum pH for both pollutants (NO<sub>3</sub><sup>-</sup> and SO<sub>4</sub><sup>2-</sup>) was found to be 7. Maximum adsorption was attained at acidic pH for CV and EY but at strong alkaline pH for OR. At lower pH, the adsorbent and cationic dyes develop strong columbic repulsions, whereas at higher pH repulsive forces were weakened by deprotonated amino groups of the sorbent [1]. The increased adsorption of CV dye at higher pH is due to increase in electrostatic attraction among the positively charged functional groups on CV and the negatively charged surface of NiGs. Higher pH values with more OH<sup>-</sup> ions compete with the anionic bromide groups of EY for the adsorption sites [28]. In the present study, the availability of adsorption sites for anionic

dye EY decreases significantly due to the binding of  $\text{OH}^-$  at higher pH. Adsorption of OR by NiGs decreased with increase in pH and the highest adsorption was achieved at pH 3. The maximum pollutant removal occurred at pH 7 and the corresponding adsorption capacities were 94% and 96% for  $\text{NO}_3^-$  and  $\text{SO}_4^{2-}$  respectively. This is in agreement with the finding of Uzair *et al.* [29] regarding the removal of  $\text{NO}_3^-$  and  $\text{SO}_4^{2-}$  by iron and nickel oxide nanoparticles from industrial waste water.

**Figure 7 : UV-Vis absorption spectra of aqueous dyes (a) CV (b) EY and (c) OR at different pH**



### Effect of NiGs dose

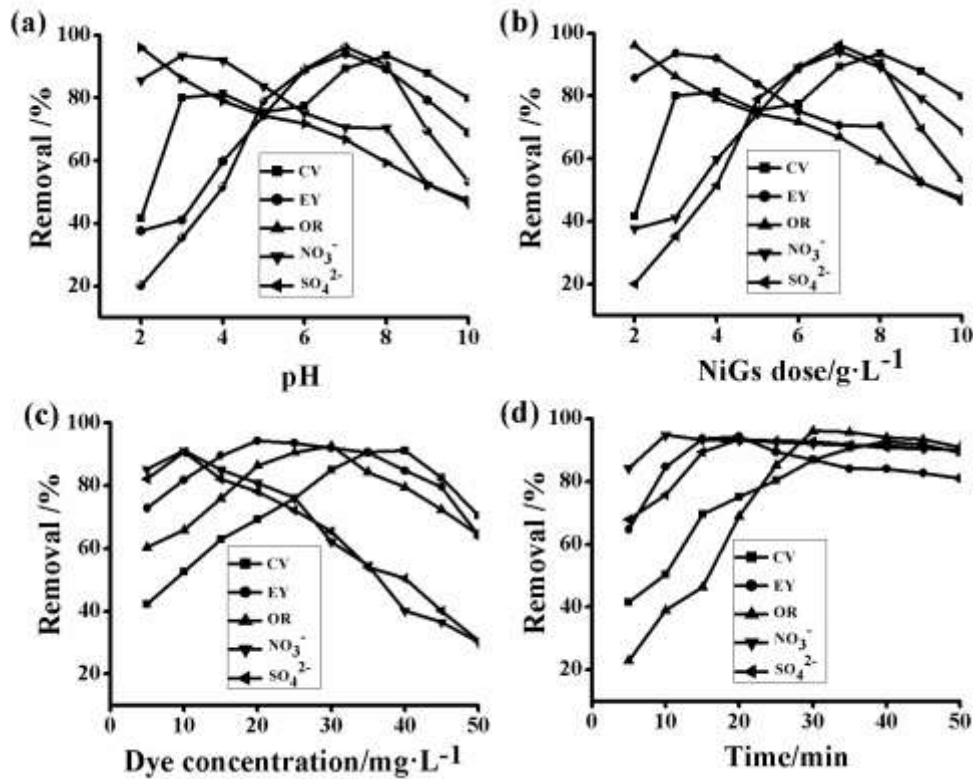
Adsorption capacity and the availability of binding sites can be determined by adsorbent dosage. The effect of NiGs dosage on the dye and pollutant adsorption was studied at  $(25 \pm 1)^\circ\text{C}$  by increasing adsorbent concentration from  $0.1$  to  $1 \text{ g}\cdot\text{L}^{-1}$  with constant adsorbate concentration of  $10 \text{ mg}\cdot\text{L}^{-1}$  for 30 min contact time. This is evident from the Fig. 8(b), where the adsorption capacity increases with increase in NiGs concentration. Adsorption percentage increased from 48% to 92% for CV, 39% to 94% for EY, 21% to 91% for OR, 32% to 95% for  $\text{NO}_3^-$  and 31% to 94% for  $\text{SO}_4^{2-}$ . This is due to increased availability of NiGs surface area for adsorption, as reported by Ahmed [30].

### Effect of initial dye and pollutant concentration

The effect of initial dye and pollutant concentrations in the range between  $5$  and  $50 \text{ mg}\cdot\text{L}^{-1}$  on adsorption capacity were shown in Fig. 8(c). Increase in adsorption percentage with increase in dye and pollutant concentration is due to the increased availability of adsorbate around the active sites of the NiGs and also due to the driving force from concentration gradient. It is evident from Fig. 8(c) that further increase in dye or pollutant concentration leads to the decrease in adsorption by NiGs. Hence, in accordance with the results obtained by El-Sayed

[31], the increase in concentration gradient with increase in dye or pollutant concentration has contributed to increased adsorption till the system reaches equilibrium. Equilibrium was obtained at initial concentrations of  $40$ ,  $20$ ,  $30$ ,  $10$  and  $10 \text{ mg}\cdot\text{L}^{-1}$  for CV, EY, OR,  $\text{NO}_3^-$  and  $\text{SO}_4^{2-}$  respectively. Above the equilibrium concentrations, the adsorption sites in NiGs were saturated and the excess dyes and pollutants remained in the solution and decreased the percentage of adsorption.

**Fig. 8.** Effect of (a) pH, (b) NiGs dose, (c) initial dye or pollutant concentration and d) different contact time on removal of CV, EY, OR, NO<sub>3</sub><sup>-</sup> and SO<sub>4</sub><sup>2-</sup>.



### Effect of contact time

Contact time of liquid and solid phases is an important factor to determine successful adsorption of dyes for practical application in real wastewater treatment [7]. Fig. 8(d) shows the effect of contact time on percentage removal of CV, EY, OR, NO<sub>3</sub><sup>-</sup> and SO<sub>4</sub><sup>2-</sup> by NiGs in aqueous solution. The adsorption percentage increased with contact time and reached equilibrium after 40, 20, 30, 10 and 20 min for CV, EY, OR, NO<sub>3</sub><sup>-</sup> and SO<sub>4</sub><sup>2-</sup> respectively. Percentage of adsorption for both dyes and pollutants increased initially with time and was stable after attaining equilibrium with longer contact time. Constantin *et al.* [32] have reported that the contact time increases availability of reactive sites while further increase in contact time cause immobilization of cationic dyes onto manganese, magnesium, cobalt and nickel magnetic nanoparticles. At initial stage, the rate of adsorption was higher, due to the availability of more reactive sites on the surface area of NiGs and becomes stable at later stages of contact time, due to lesser number of active sites that lead to immobilization of dye on nanoparticles.

### Adsorption isotherms

#### Langmuir isotherm

The Langmuir isotherm is suitable for monolayer adsorption onto a surface containing a finite number of identical sites and is represented by the Eq. (4) [32].

$$C_e/q_e = C_e/q_m + 1/K_L q_m \quad (4)$$

where  $q_m$  (mg·g<sup>-1</sup>) and  $K_L$  (L·mg<sup>-1</sup>) are Langmuir constants that represents maximum adsorption capacity and energy of adsorption respectively.  $q_e$  values of dyes and pollutants were determined by Eq. (2). The

experimental data  $C_e/q_e$  were plotted against  $C_e$  and are shown in Fig. 9(a). Maximum adsorption per unit of the adsorbent ( $q_m$ ) and Langmuir constant ( $K_L$ ) were determined from the plot (intercept and slope).

An important parameter in Langmuir is the separation factor  $R_L$  that indicates the nature of isotherm to be unfavorable ( $R_L > 1$ ), linear ( $R_L = 1$ ), favorable ( $0 < R_L < 1$ ), or irreversible ( $R_L = 0$ ) [33] and is represented by the Eq. (5) [8]:

$$R_L = 1 / (1 + (K_L C_e)) \quad (5)$$

Parameters and correlation coefficients ( $R^2$ ) obtained from the plots of Langmuir ( $C_e/q_e$ ) are shown in Table 1. The  $R^2$  values were found to be 0.976, 0.955, 0.864, 0.935 and 0.784 for CV, EY, OR,  $NO_3^-$  and  $SO_4^{2-}$  respectively.  $R_L$  values for all the dyes and pollutants were between 0 and 1 indicating favorable adsorption for adsorbates. Higher correlation coefficients ( $R^2$ ) in Langmuir isotherm confirmed that the surface of NiGs can accommodate a monolayer of adsorbate without any interaction between adsorbed species. A similar trend was also reported by Mantosh and Priya [33] for dyes and by Jolly *et al.* [34] for pollutants.

**Freundlich isotherm**

Freundlich isotherm was used to describe the adsorption characteristics of multilayer and heterogeneous surfaces with unequally available adsorption sites that have different adsorption.

$$\lg q_e = \lg K_F + (1/n) \lg C_e \text{-----(6)}$$

where  $K_F$  ( $mg \cdot g^{-1}$ ) and  $n$  are Freundlich constants related to adsorption capacity and adsorption intensity respectively. Freundlich isotherm was determined by plotting the experimental data  $\log q_e$  against  $\log C_e$  and is shown in Fig. 9(b).  $K_F$  and  $n$  were calculated from the intercept and the slope value of the plot.  $K_F$  value showed that the rate of adsorption increased in later stages of contact time.  $n$  value between  $1 < n < 10$  illustrated that adsorbate was favorable adsorbed on NiGs. Higher  $n$  values (2.898, 5.524, 2.597, 9.523 and 5.128 for CV, EY, OR,  $NO_3^-$  and  $SO_4^{2-}$  respectively) in Table 1 showed stronger adsorption intensity. Higher  $R^2$  values in Langmuir than Freundlich isotherm suggest that adsorption of dyes and pollutants onto NiGs followed the Langmuir model.

**Fig. 9. (a) Langmuir isotherm plot and (b) Freundlich isotherm plot for adsorption of CV, EY,OR,  $NO_3^-$  and  $SO_4^{2-}$  onto NiGs**

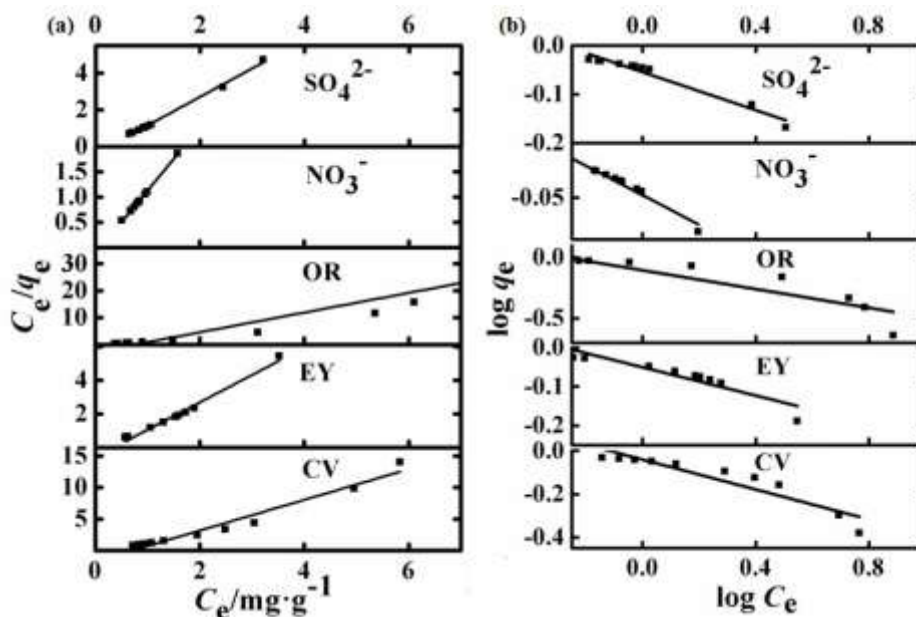


**Table 1 Adsorption isotherms for removal of dyes and pollutants by NiGs at different contact time**

Adsorbate	Langmuir isotherm			Freundlich isotherm			Dubinin–Radushkevich isotherm				
	$q_m$ /mg·g <sup>-1</sup>	KL/L·mg <sup>-1</sup>	RL	R2	$K_F$ /mg·g <sup>-1</sup>	$n$	R2	qR /mmol·g <sup>-1</sup>	BDR	E	R2
CV	0.454	1.692	0.055	0.961	0.040	2.898	0.873	0.542	1.00E-07	2.236	0.592
EY	0.615	0.566	0.638	0.982	0.050	5.524	0.846	0.266	4.00E-08	3.535	0.549
OR	0.273	2.738	0.267	0.866	0.105	2.597	0.810	0.734	8.00E-08	2.500	0.492
NO <sub>3</sub> <sup>-</sup>	0.795	0.130	0.884	0.998	1.096	9.523	0.952	0.168	2.00E-08	5.000	0.803
SO <sub>4</sub> <sup>2-</sup>	0.645	0.390	0.719	0.995	1.090	5.128	0.873	0.326	5.00E-08	3.162	0.802

### Dubinin–Radushkevich (D–R) isotherm

The D–R isotherm describes the type of adsorption process that can either be physical or chemical adsorption and it assumes that the surface is heterogeneous [8]. The linear form of Dubinin–Radushkevich is represented by the Eq. (7) [8]:

$$\ln(q_e) = \ln q_{DR} - B_{DR} \varepsilon^2 \quad (7)$$

where  $B_{DR}$  (mol<sup>2</sup>·J<sup>-2</sup>) and  $q_{DR}$  (mmol·g<sup>-1</sup>) are D–R constants related to adsorption energy and adsorption capacity respectively.  $\varepsilon$  is the Polanyi potential related to adsorption energy and is represented as the Eq. (8) [8]:

$$\varepsilon = RT \ln(1+1/C_e) \quad (8)$$

where  $R$  is the universal gas constant (8.314 J·mol<sup>-1</sup>·K<sup>-1</sup>) and  $T$  is the absolute temperature in Kelvin. Mean free energy of adsorption  $E$  (KJ·mol<sup>-1</sup>) is represented by the Eq. (9) [8]:

$$E = 1/\sqrt{2B_{DR}} \quad (9)$$

The value of  $E$  estimates the nature of adsorption. If  $1 < E$  (KJ·mol<sup>-1</sup>)  $< 8$ , the physical adsorption becomes a dominant process while if  $8 < E$  (KJ·mol<sup>-1</sup>)  $< 16$ , the chemical adsorption becomes a dominant process [8]. The constants of D-R equation were obtained from the slope and intercept of the plots in Fig. 10. As mentioned in the Table 1, mean energy ( $E$ ) values of 2.236, 3.535, 2.500, 5.000 and 3.162 kJ·mol<sup>-1</sup> for CV, EY, OR, NO<sub>3</sub><sup>-</sup> and SO<sub>4</sub><sup>2-</sup> respectively were between 1 and 8 suggesting physical adsorption of these adsorbate onto NiGs.

### Adsorption kinetics

Adsorption kinetics explains the rate of uptake of adsorbate by NiGs and predicts the residence time of dyes and pollutants at the solid-liquid interface as reported by Mantosh and Priya [33].

### Pseudo-first-order kinetics

The adsorption kinetics of CV, EY, OR, NO<sub>3</sub><sup>-</sup> and SO<sub>4</sub><sup>2-</sup> onto NiGs were investigated by Lagergren's pseudo-first-order and is represented as follows in the Eq. (10) [17].

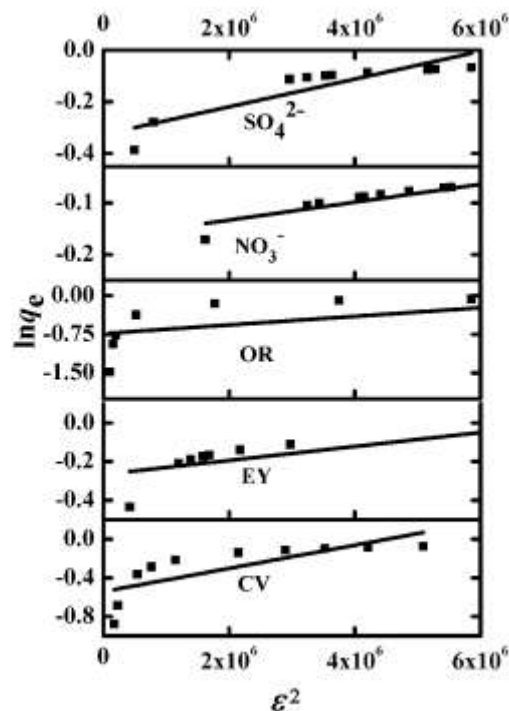
$$\lg(q_e - q_t) = \lg q_e - (K_1 t / 2.303) \quad (10)$$

where  $q_e$  and  $q_t$  in mg·g<sup>-1</sup> are the amount of dyes or pollutants adsorbed at equilibrium and at a specific time respectively.  $K_1$  (min<sup>-1</sup>) is the pseudo-first-order rate constant calculated from the plots of  $\log(q_e - q_t)$  versus  $t$

and is shown in Fig .11(a). Correlation coefficient ( $R^2$ ) was also calculated from the plot. Parameters of pseudo-first-order kinetics were listed in Table 2.

Pseudo-first-order model indicates the rate of occupation of adsorption sites is proportional to the number of unoccupied sites [9]. The  $R^2$  values also shows that the adsorption of dyes and pollutants onto NiGs do not follow pseudo-first-order kinetics. Furthermore, the wide variation in  $q_e$  values also confirmed that the pseudo-first-order kinetics is not appropriate model for relating adsorption of CV, EY, OR,  $\text{NO}_3^-$  and  $\text{SO}_4^{2-}$  onto NiGs. Mantosh *et al.* [33] also reported similar results with CV on silver-nanocomposites.

**Fig. 10. Dubinin–Radushkevich plot for adsorption of CV, EY, OR,  $\text{NO}_3^-$  and  $\text{SO}_4^{2-}$  onto NiGs.**



### Pseudo-second-order kinetics

Kinetic data were further examined by Ho and McHay pseudo-second-order kinetics [18] and are represented as follows in the Eq. (11):

$$t/q_t = 1/K_2 q^2 + t/q \quad (11)$$

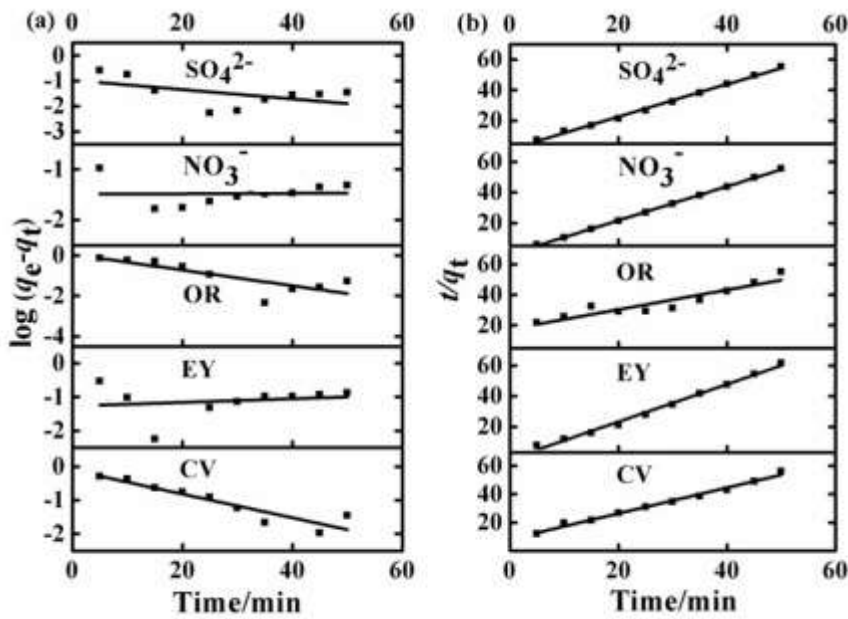
where  $K_2$  ( $\text{g}\cdot\text{mg}^{-1}\cdot\text{min}^{-1}$ ) is the rate constant of pseudo-second-order reaction determined from plot of  $t/q_t$  versus  $t$  and is shown in the Fig. 11(b). Table 2 shows the kinetic data of pseudo- second-order models.

Higher values of  $R^2$  and shape of the line in the plot showed excellent fit of pseudo-second-order kinetics. The kinetics data suggest that the adsorption process depends on both the adsorbate and adsorbent. It is evident from the Table 2 that adsorption of both dyes and pollutants onto NiGs obey pseudo-second-order kinetics. Similar phenomenon was recorded for acid blue dye adsorption onto modified diatomite by Khalighi *et al.* [2] and for anionic pollutants adsorption by Hossain *et al.* [35].

Table 2 Kinetics data for removal of dyes and pollutants by NiGs

Dyes & Pollutants	Pseudo- first-order kinetics			Pseudo-second-order kinetics		
	$K_1/\text{min}^{-1}$	$q_e/\text{mg}\cdot\text{g}^{-1}$	R2	$K_2/\text{g}\cdot\text{mg}^{-1}\cdot\text{min}^{-1}$	$q_e/\text{mg}\cdot\text{g}^{-1}$	R2
CV	0.026	0.210	0.380	8.315	1.103	0.989
EY	0.012	0.453	0.167	1.212	0.816	0.993
OR	0.037	0.121	0.518	17.49	1.557	0.871
NO <sub>3</sub> <sup>-</sup>	0.012	0.993	0.125	0.406	0.902	0.999
SO <sub>4</sub> <sup>2-</sup>	0.023	0.703	0.248	1.175	0.935	0.997

Fig. 11. (a) Pseudo-first-order kinetic and (b) Pseudo-second-order kinetic plot for adsorption of CV, EY, OR, NO<sub>3</sub><sup>-</sup> and SO<sub>4</sub><sup>2-</sup> onto NiGs.



## Conclusion

Nickel nanoparticles were synthesized from the leaf extracts of *Raphanus Sativus*. The UV–Vis absorption peak was monitored at 395 nm. FTIR spectra of the synthesized nanoparticles display peaks characteristic for functional groups like N–H, C–N, C–H and O–H. XRD pattern confirmed the fcc structure of nickel nanoparticles. Microscopic studies by SEM and TEM showed the morphology of synthesized NiGs was almost spherical in shape and the size of the NiGs was between 12 and 36 nm. This adsorption study suggest that the NiGs was efficient in the removal of cationic, anionic, azo dyes (CV, EY, OR) and anionic pollutants ( $\text{NO}_3^-$ ,  $\text{SO}_4^{2-}$ ) from aqueous solutions. Langmuir isotherm model fitted better to the adsorption of CV, EY, OR,  $\text{NO}_3^-$  and  $\text{SO}_4^{2-}$  onto NiGs at all stages of contact time which further evidences monolayer adsorption. Mean free energy of adsorption ( $E$ ) obtained from D–R isotherm model suggest physical adsorption of adsorbates onto NiGs. The kinetics data were better fitted to pseudo- second-order kinetics model. The present study concludes that NiGs is an economical, eco- friendly and efficient adsorbent for removal of hazardous anionic pollutants and dyes from aqueous solution.

## References:

1. Mona, S., Soheir, A.K., Amina, A.A., “Basic Dye Adsorption on Low Cost Biopolymer: Kinetic and Equilibrium Studies”, *J. Appl. Chem.*, 4(2), 27–36 (2012).
2. Khalighi, S.R., Khosravi, M.R., Badii, K.H., Yousefi, L., “Adsorption of Acid Blue 92 dye on modified diatomite by Nickel oxide nanoparticles in aqueous solution”, *Prog. Color. Colorants Coat.*, 5, 101-116 (2012).
3. Akan, J.C., Moses, E.A., Ogugbuaja, V.O., Abah, J., “Assessment of Tannery Industrial Effluents from Kano Metropolis, Kano State, Nigeria”, *J. Appl. Sci.*, 7(19), 2788-2793 (2007).
4. Roya, N., Gholam, R.B., Mohammad, M.A., Hamed, M., “Decolourization of synthetic wastewater by Nickel oxide nanoparticles”, *Int. J. Env. Health Eng.*, 1(1), 1-25 (2013).
5. Reza, K.S., Mohammad, R.K.N., Khashayari, B., Nargess, Y.L., Gelayol, G., “Equilibrium and kinetics studies for the adsorption of Basic Red 46 on nickel oxide nanoparticles-modified diatomite in aqueous solutions”, *J. Taiwan Inst. Chem. Eng.*, 45, 1792-1802 (2014).
6. Reza, K.S., Mohammad, R.K.N., Khashayar, B., Soroush, M., “Evaluation of adsorption kinetics and equilibrium for the removal of benzene by modified Diatomite”, *Chem. Eng. Technol.*, 36, 1713-1720 (2013).
7. Reza, K.S., Saeed, A., Mohammad, R.K.N., Khashayar, B., Mohammad, S.S., “Liquid Phase adsorption kinetics and equilibrium of toluene by novel modified-diatomite”, *J. Environ. Health Sci. Eng.*, 12, 1-13 (2014).
8. Saeed, A., Ali, R.K., Mohammad, A.M., “Sorption of heavy metal ions from aqueous solution by a novel cast PVA/TiO<sub>2</sub> nanohybrid adsorbent functionalized with amine groups”, *J. Ind. Eng. Chem.*, 20, 1656–1664 (2014).
9. Subramani, S., Thirumalai, D., Sarumathy, K., Vijay, T. “Synthesis of copper nanoparticles using *Raphanus Sativus* (Radish) and its application in degradation of Methylene Blue dye”, *International Journal of ChemTech Research.*, 14(1): 121 – 129 (2021).
10. Huimei, C., Jing, W., Dengpo, H., Xiaoer, C., Jiajia, Z., Daohua, S., Jiale, H., Qingbiao, L., “Plant-mediated synthesis of size-controllable Ni nanoparticles with alfalfa extract”, *Mat Lett.*, 122, 166–69 (2014).
11. Adams, E.Q., Rosenstein, L., “The color and ionization of crystal violet”, *J. Am. Chem. Soc.*, 36 (7), 1452–1473 (1914).
12. APHA. Standard methods for the examination of water and waste water, 21<sup>st</sup> edition American Public Health Association, Washington, DC (2005).
13. Rossum, J.R., Villarruz, P., “Suggested methods for turbidimetric determination of sulfate in water”, *J. Am. Water Works Assoc.*, 53, 873–876 (1961).
14. Sun, L., Wana, S., Luo, W., “Biochars prepared from anaerobic digestion residue, palm bark, and eucalyptus for adsorption of cationic methylene blue dye: Characterization, equilibrium, and kinetic studies”, *Bioresour. Technol.*, 140, 406–413 (2013).
15. Mundhe, K.S., Gaikwad, A.B., Torane, R.C., Deshpande, N.R., Kashalkar, R.V., “Adsorption of

- methylene blue from aqueous solution using *Polyalthia longifolia* (Ashoka) seed powder”, J. Chem. Pharm. Res., 4, 423–436 (2012).
16. Gurusamy, A., Lai, Y., Jiunn, F. L., “Adsorption of reactive dye from an aqueous solution by chitosan: isotherm, kinetic and thermodynamic analysis”, J. Hazard. Mater., 152, 337–346 (2008).
  17. Ho, Y. S., McKay, C., “Pseudo second order model for sorption processes”, Proc. Biochem., 34, 451–465 (1999).
  18. Kazem, N., Elias, S., Khadijeh, R., Wan, M.M.Y., “Influence of dose on particle size of colloidal silver nanoparticles synthesized by gamma radiation”, Radiat. Phys. Chem., 79, 1203–1208 (2010).
  19. Abdo M.M., Elham, G., Nayereh, S., Wan, M.M.Y., Elias, S., “Structural, optical and electrical properties of PVA/PANI/Nickel nanocomposites synthesized by gamma radiolytic method”, Polymers, 6, 2435-2450 (2014).
  20. Khalid, N., Munetaka, O., Raquel, D., Mohammed, A., Kityk, I.V., Mosto, B., “Nanoscale synthesis and optical features of metallic nickel nanoparticles by wet chemical approaches”, J. Alloys Comps., 509, 5882–5886 (2011).
  21. Evanoff, D.D., Chumanov, G., “Synthesis and optical properties of silver nanoparticles and arrays”, Chem. Phys. Chem. 6, 1221-1223 (2005).
  22. Mallikarjuna, K., Narasimha, G., Dillip, G., Praveen, B., Shreedhar, B., Sreelakshmi, C., Reddy, B., Deva, P., “Green synthesis of silver nanoparticles using *Ocimum* leaf extract and their characterization”, Dig. J. Nanomater. Biostruct., 6: 181–186 (2011).
  23. Sathyavathi, R., Krishna, M. B., Rao, S. V., Saritha, R., Rao, D. N., “Biosynthesis of silver nanoparticles using *Coriandrum sativum* leaf extract and their application in non-linear optics”, Adv. Sci. Lett., 3 (2), 138–143 (2010).
  24. Hou, Y., Kondoh, H., Ohta, T., Gao, S., “Size-controlled synthesis of nickel nanoparticles”, Appl. Surf. Sci., 241, 218–221 (2005).
  25. Govindasamy, R., Jeyaraman, R., Kadarkaraitangam, J., Arumugam, M., Gandhi, E., Chinnaperumal, K., Thirunavukkarasu, S., Sampath, M., Abdul, A. Z., Asokan, B., Chidambaram, J., Arivarasan, V.K., Moorthy, I., Chinnadurai, S., “Novel and simple approach using synthesized nickel nanoparticles to control blood-sucking parasites”, Vet. Parasitol. 191, 332-339 (2013).
  26. Wang, X, S., Liu, X., Wen, L., Zhou, Y., Li, Z., “Comparison of basic dye crystal violet from aqueous solution by low-cost biosorbents”, Sep. Sci. Technol., 43, 3712–3731 (2008).
  27. Shahla, E., Maryam, A., Ladan, E., “Preparation and characterization of Diethylentriamine - montmorillonite and its application for removal of Eosin Y dye: Optimization, kinetic and isotherms study”, J. Sci. Ind. Res., 72, 461–466 (2013).
  28. Uzaire, R., Arun, I., Abida, K., “Synthesis, characterization and application of nanomaterials for the removal of emerging pollutants from industrial waste water, kinetics and equilibrium model”, J. Water Sustain., 2, 233-244 (2012).
  29. Ahmed, R., “Studies on adsorption of crystal violet from aqueous solution onto coniferous pinus bark powder”, J. Hazard. Mater., 171, 767-773 (2009).
  30. El-Sayed., “Removal of methylene blue and crystal violet from aqueous solutions by palm kernel fiber”, Desalination., 272, 225–232 (2011).
  31. Constantin, V., Radu, G.S., Tiberiu, R., Daniel, G., Nicoleta, C., Aurel, P., “Studies on the adsorption capacity of cationic dyes on several magnetic nanoparticles”, Acta Chemica Iasi., 21, 19–30 (2013).
  32. Mantosh, K.S., Priya, B., “Plant-mediated synthesis of silver-nanocomposite as novel effective azo dye adsorbent”, Appl. Nanosci. 5(1), 1-9 (2013).
  33. Jolly, P., Manas, K., Dhananjay, K., Deshmukh., “Removal of methyl orange by activated carbon modified by silver nanoparticles”, Appl. Water Sci., 3, 367-374 (2013).
  34. Hossain, M.A., Kumita, M., Michigami, Y., Mori, S., “Kinetics of Cr (VI), Adsorption on used black tea leaves”, J. Chem. Eng. Jpn., 38(6), 402-406 (2005).

\*\*\*\*\*